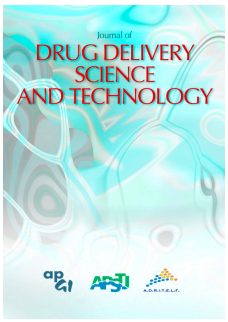

Different instrumental approaches to understand the chitosan coated niosomes/mucin interaction

Federica Rinaldi, Patrizia Nadia Hanieh, Anna Imbriano, Daniele Passeri, Elena Del Favero, Marco Rossi, Carlotta Marianecci, Simone De Panfilis, Maria Carafa

PII: S1773-2247(19)31336-X

DOI: https://doi.org/10.1016/j.jddst.2019.101339

Reference: JDDST 101339

To appear in: *Journal of Drug Delivery Science and Technology*

Received Date: 5 September 2019

Revised Date: 15 October 2019

Accepted Date: 19 October 2019

Please cite this article as: F. Rinaldi, P.N. Hanieh, A. Imbriano, D. Passeri, E. Del Favero, M. Rossi, C. Marianecci, S. De Panfilis, M. Carafa, Different instrumental approaches to understand the chitosan coated niosomes/mucin interaction, *Journal of Drug Delivery Science and Technology* (2019), doi: https://doi.org/10.1016/j.jddst.2019.101339.

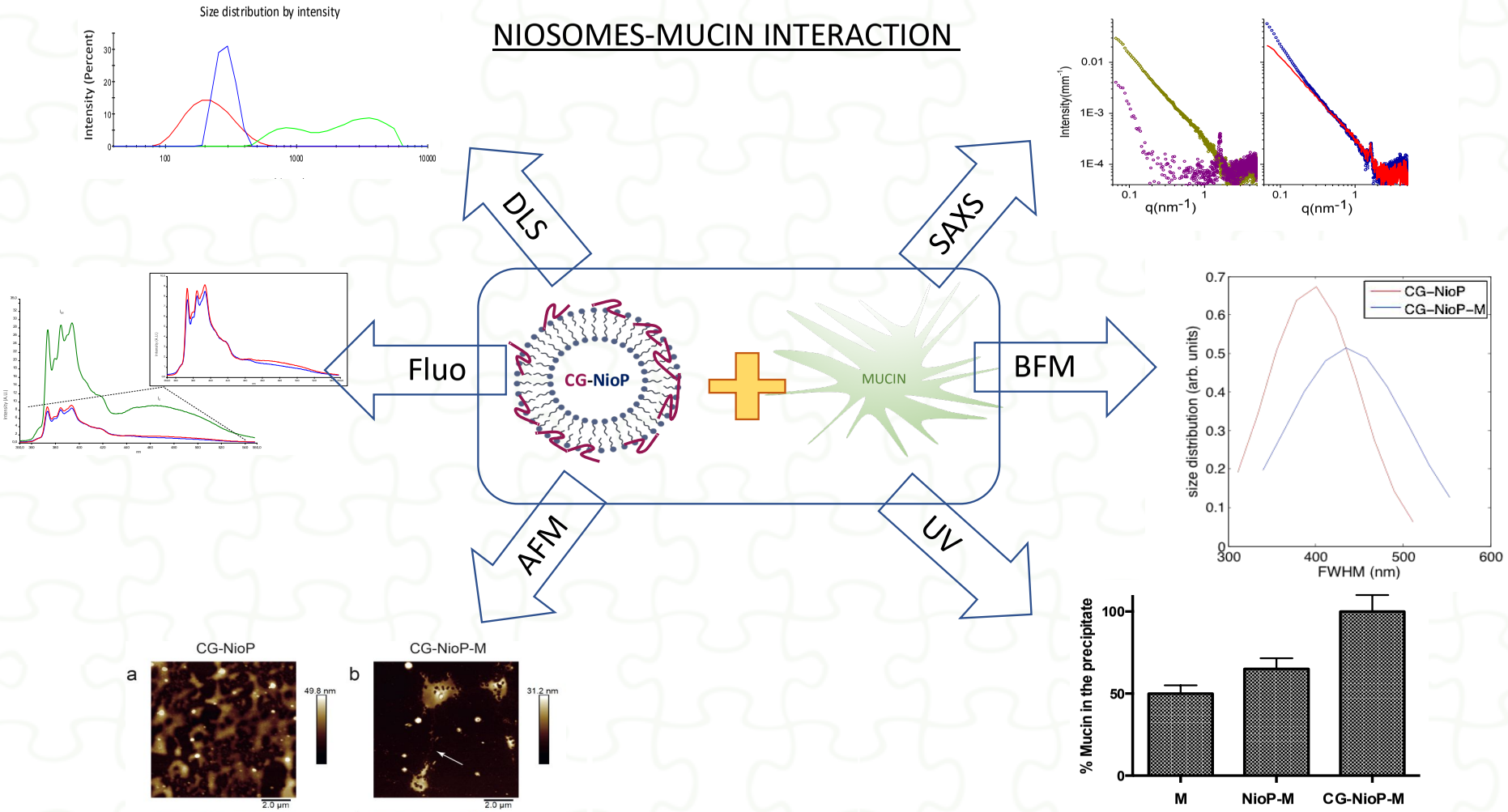
NIOSOMES-MUCIN INTERACTION
Size distribution by intensity
Intensity (Percent)
DLS
SAXS
Intensity(mm-1)
q(nm-1)
Fluo
CG-NioP
MUCIN
BFM
CG–NioP
CG–NioP–M
size distribution (arb. units)
FWHM (nm)
AFM
UV
CG-NioP
CG-NioP-M
a
b
49.8 nm
31.2 nm
2.0 µm
% Mucin in the precipitate
M
NioP-M
CG-NioP-M

Different instrumental approaches to understand the chitosan coated niosomes/mucin interaction.

Federica Rinaldi[a], Patrizia Nadia Hanieh[b], Anna Imbriano[b], Daniele Passeri[c], Elena Del Favero[d], Marco Rossi[c], Carlotta Marianecci[b]*, Simone De Panfilis[a], Maria Carafa[b]

[a] Center for Life Nano Science@Sapienza, Istituto Italiano di Tecnologia (ITT), Viale Regina Elena 291, 00161 Rome, Italy; federica.rinaldi@iit.it, simone.depanfilis@iit.it.

[b] Department of Drug Chemistry and Technology, Sapienza University of Rome, P.zzle A. Moro 5, 00185 Roma, Italy; patrizianadia.hanieh@uniroma1.it; anna.imbriano@uniroma1.it; carlotta.marianecci@uniroma1.it; maria.carafa@uniroma1.it.

[c] Department of Basic and Applied Sciences for Engineering, Sapienza University of Rome, Via A. Scarpa 14, 00161 Rome, Italy; daniele.passeri@uniroma1.it; marco.rossi@uniroma1.it.

[d] Department of Medical Biotechnology and Translational Medicine, University of Milan, V.le F. lli Cervi 93, 20090 Segrate, Italy; elena.delfavero@unimi.it.

* Corresponding author: Carlotta Marianecci, Department of Drug Chemistry and Technologies, Sapienza University of Rome, Piazzale A. Moro 5, Rome 00185, Italy. E-mail address: carlotta.marianecci@uniroma1.it

Abstract

Span-20 non-ionic surfactant vesicles (niosomes), designed for future applications in brain drug delivery through intranasal route, are prepared and coated with chitosan glutamate, a mucoadhesive agent specifically proposed for brain delivery and for an optimal interaction with nasal mucin, with the aim to promote the vesicles residence time in the nasal cavity. The understanding of the interaction between chitosan coated niosomes with mucin is of great relevance as it can influence their in vivo distribution and physiological behaviour. Complementary and different techniques are then used in a non-conventional combined approach to study this phenomenon. The integrated use of dynamic light scattering (DLS), fluorimetric and spectrophotometric assays, small-angle X-ray scattering (SAXS), atomic force microscopy (AFM) and high speed brightfield microscopy (BFM) allows to shed new light on the physico-chemical behaviour of the mucin-niosomes system, addressing this complex phenomenon by different perspectives.

Keywords

Niosomes, mucoadhesion, AFM, SAXS, BFM and DLS.

1. Introduction

Every technique possesses particular features that can be combined or compared to others to address the overall nanocarriers properties.

In a classical characterization approach, a specific technique is applied to study a distinct parameter: e.g. Small angle x-ray scattering (SAXS) [1] is used to determine with high accuracy size and bilayer features of vesicles; atomic force microscopy (AFM) [2] is applied to provide textural information on nanocarriers; high speed brightfield microscopy (BFM) [3, 4] is commonly used to study cell-nanocarrier interactions; dynamic light scattering (DLS) is able to provide dimensions and ζ-potentials of particles dispersed in a fluid [5]. Furthermore fluorimetric and spectrophotometric techniques are usually applied in pharmaceutics to provide probe/drug quantitative analyses, as in release studies. Here, in a less conventional approach, all these techniques are used in a combined way, out of their usual application field, to study the interaction between chitosan coated niosomes and mucin.

Niosomes (non-ionic surfactant vesicles) are vesicular systems with nanometric dimensions, characterized by an aqueous core and lipophilic bilayer. They are composed by a non-ionic surfactant (e.g. Span 20) coupled together with cholesterol. They are able to entrap and deliver both lipophilic and hydrophilic drugs or probes and the potential to modulate both their pharmacokinetic and pharmacodynamic profiles, thereby enhancing their therapeutic index. Vesicles increase drug in vivo stability, extend its blood circulation time, and allow controlled drug release obtaining a specific biodistribution of drugs reducing side effects. Although only a few niosomal formulations are in clinical trials, and no formulations are in the commercial market, their several advantages, including also low toxicity, high chemical stability, and lower manufacturing cost, provided the opportunity to develop a niosomal medicine product for brain delivery.

To obtain niosomal formulations able to carry out nose-to-brain delivery, some factors must be taken in account. In particular, to enhance the niosomal residence time in nasal cavity, a mucoadhesive agent must be added. Chitosan is a biodegradable and bioadhesive polymer able to interact with the mucin in nasal cavity thanks to electrostatic interactions. Chitosan prolongs residence time in the nasal cavity of drugs and/or formulations, allowing drug delivery systems to promote

drug absorption In recent studies chitosan glutamate (CG) is also proposed as a better mucoadhesive agent than chitosan or chitosan salts [6-8]. To this aim, CG is used to coat niosomes, obtaining CG-niosome complexes, to confer mucoadhesive properties to the formulation, able to be successfully used for intranasal applications. Of course, the physical-chemical properties of these CG-niosome complexes affect their in vivo distribution and physiological behaviour and must be properly characterized to better understand their efficacy as intranasal drug carriers.

The aim of this work is to use different techniques [9] to study the interaction between mucin and chitosan-glutamate-niosomes loaded with model drug (CG-NioP), to this aim, DLS [10], fluorometric and spectrophotometric assays, SAXS, AFM and BFM have been employed.

2. Materials and Methods

2.1. Materials

HEPES salt (Sodium 2-(4-(2-hydroxyethyl) piperazin-1-yl) ethanesulfonate), cholesterol, Sephadex G75, model drug (pentamidine isethionate), pyrene, mucin from porcine stomach type II powder, Span 20 (Sorbitan monolaurate), chitosan medium molecular weight powder (C) and sodium hydroxide were purchased from Sigma-Aldrich (Milan, Italy). L-Glutamic acid (G) was supplied by PanReac Applichem (Milan, Italy). All other products and reagents were of analytical grade.

2.2. Methods

2.2.1. Niosome Preparation and Purification

Niosomes were prepared using thin film hydration method [8, 10]. Span 20 (15 mM) and cholesterol (15 mM) were dissolved in organic solvent mixture (chloroform/methanol 3:1 v/v). The solvent was evaporated using rotary evaporator (VV2000, Heidolph, Schwabach, Germany) to form a thin “film” at the temperature of 60 °C. The lipophilic components, such as Pyrene, were solubilized with organic solvents together with cholesterol and surfactant, while the hydrophilic components, such the model drug, were added during the hydration step. In particular, the film was hydrated using 5 mL of model drug solution (0,5 mg/mL in HEPES buffer 0.01 M, pH 7.4), vortexed and sonicated at

60 °C and 18% amplitude for 15 min using ultrasonic microprobe (Vibra-Cell VCX-400, Sonics & Materials, Newtown, CT, USA). The unilamellar vesicle suspension was purified by gel filtration chromatography using Sephadex G75 (glass column of 50 × 1.2 cm) with HEPES buffer as the eluent. The obtained purified vesicles were filtrated by using cellulose filters with pore diameter of 1.2 μm, to purify the niosomal suspension and obtain desired dimensions.

2.2.2. Preparation of Chitosan Glutamate-Coated Niosomes with model drug

Chitosan glutamate solution was prepared by dissolving C (1 mg) and G (0.82 mg) in acetate buffer (0.2 M, pH 4.4) up to a final concentration of 0.05 mg/mL [11]. The obtained solution was stirred overnight [12]. CG coating of model drug loaded niosomes (NioP) was obtained by adding a CG solution to vesicular suspension into a 1:1 ratio [13]. The obtained suspension was stirred for 1 h at room temperature to achieve CG-coated model drug niosomes (CG-NioP). pH values were measured and confirmed for all formulations to match a suitable pH for nasal administration ($3.5 < pH < 6.4$).

2.2.3. Preparation of Mucin Solution and Mucoadhesive Studies

Mucin powder was dissolved in HEPES buffer to produce a mucin solution (2 mg/mL, pH 6) and stirred overnight at 34°C [14]. Specific parameters, including temperature (30°C), concentration of mucin (2 mg/mL) and pH value (6.3–6.7), were analysed in the mucoadhesive study to mimic the conditions in the nasal mucosal site [15]. Mucin solutions (2 mg/mL) were mixed with CG-NioP suspensions (1:1 ratio) and incubated at 30°C [15, 16]. The concentration of mucin solutions employed in this study was modified to obtain optimal pH value (6.3–6.7) [15, 17].

2.2.4. DLS

Uncoated niosomes with model drug, CG-NioP and mixture of CG-NioP with mucin (CG-NioP-M) were analysed and their particle diameter, polydispersity index (PDI) and ζ-potential were measured in HEPES buffer by dynamic light scattering using a Zetasizer (Nano ZS90, Malvern, UK) (n= 3 repeated

158 measurements for each sample) [10]. Particle size and ζ-potential were
159 measured at 0, 5, 10, and 15 min, to determine the time-course of uncoated and
160 coated niosome-mucin interaction and the stability of the obtained complex.
161 Results related to the data collected at 15 min were considered (in order to
162 mimic the *in vivo* interaction time of intranasal administration) even when the
163 interaction was already almost complete after only 5 min. Mucoadhesive
164 measurements were carried out expressing particle dimension as hydrodynamic
165 diameter and evaluating also the different curves related to size distribution by
166 intensity to better appreciate the formation of complex between CG-NioP and
167 mucin, in order to avoid artefacts due to the potential mucin aggregates.
168
169 *2.2.5. Fluorimetry*
170 Interactions by CG-NioP and mucin were also evaluated by fluorescence
171 turbidity measurements using luminescence spectrometer (LS5013,
172 PerkinElmer, Waltham, MA, USA) at Ex/Em 600/600 nm [16]. Bilayer
173 characterization was carried out on NioP, CG-NioP and CG-NioP-M. Due to its
174 lateral diffusion within the bilayer, pyrene provides a wider picture of the bilayer
175 characteristics, such as microviscosity and polarity [18]. By fluorescent
176 techniques the behaviour inside bilayer and the expected interaction between
177 mucin and the bilayer were evaluated. Pyrene loaded niosomes were prepared
178 by adding pyrene (4 mM) with other vesicle components (same preparation
179 method as above). The lateral distribution and the mobility of membrane
180 compounds can be studied by fluorescence measurements. Pyrene is a
181 florescence probe; whose monomer exhibited a spectrum characterized with five
182 emission peaks (from I_1 to I_5) and excimer has only one peak (I_E). Pyrene can
183 form intramolecular excimer based on the viscosity of the probe
184 microenvironment [19]. The fluorescence signals emitted by pyrene loaded
185 niosomal suspension were studied by an emission spectrum (λ = 350–550 nm)
186 using and Ex= 330 nm by a luminescence spectrometer (LS5013, PerkinElmer)
187 [20].
188
189 *2.2.6. Spectrophotometry*
190 a) Mucoadhesive strength was determined by the method proposed by Sandri et
191 al. [21] The percent binding efficiency of niosomes to mucin was determined by

mixing 1 ml of porcine mucin suspension (2 mg/ml in Hepes buffer) with the same volume of CG-NioP or NioP. The mucin alone and then the mixture with niosomal suspensions were then centrifuged at 18000 rpm for 30 min at temperature of 4°C. The concentration of free mucin in the supernatant was determined at 255 nm using UV spectrophotometer (Perkin-Elmer lambda 25 UV/Vis). The mucin binding efficiency of CG-NioP was calculated from the following equation:

$$\text{Mucin binding efficiency } (\%) = \frac{\text{Total mucin} - \text{Free mucin}}{\text{Total mucin}} \text{x } 100 \quad (1)$$

b) Aliquots of CG-NioP, NioP and CG were mixed with mucin (1:1 in volume). The effective absorbance (A) of the samples, operating at λ = 500nm, was compared to the theoretical absorbance (A_{theor}) calculated by adding the individual absorbance values of the mucin and each sample suspension (CG-NioP, NioP and CG). The difference in absorption ($\Delta A = A - A_{theor}$) was taken as a measure of the interaction between mucin and CG-NioP, NioP or CG, namely $\Delta A \cong 0$ if no interaction occurs, while if $\Delta A > 0$, a strong interaction between mucin and the analysed samples was inferred.

2.2.7. SAXS

SAXS experiments were carried out at the European Synchrotron Radiation Facility (ESRF, Grenoble, France) to obtain information on the internal structure of formulations for drug delivery [5, 21]. In the case of SAXS the intensity decay behaviour as a function of momentum transfer q ($q = (4\pi/\lambda) \sin(\theta/2)$, being θ the scattering angle) can provide knowledge on the structure of particles in solution down to the nm length scale. Measurements were acquired at the high-brilliance beamline ID02, with two sample-detector distances, in the region of momentum transfer $0.017 nm^{-1} \leq q \leq 5 nm^{-1}$. Samples were inserted in 2mm capillaries (KI-beam, ENKI, Concesio, Italy) and placed horizontally onto a thermostated sample holder (T=25 ± 0.1 °C). Very shorts frames were collected (exposure time 0.1 s) and checked for effects induced by radiation damage before being averaged. After radial integration and background subtraction, the SAXS profiles report the scattered radiation intensity as a function of momentum transfer, q.

2.2.8. AFM

Atomic force microscopy (AFM) topographical characterization were carried out using a standard AFM setup (Dimension Icon, Bruker Inc. in 'soft tapping' mode) equipped with standard silicon cantilevers (OTESPA, Bruker Inc.). A drop of solution was deposited on a 111 single-crystal silicon waiting a few minutes to allow some vesicles to adhere to the substrate. Eventually, the drop was drawn in order to prevent the deposition of excessive material, which could lead to the formation of a continuous film instead of isolated vesicles. A few minutes were further waited to allow an (incomplete) evaporation of the solvent at room conditions. Images were collected near the edge of the drops to avoid regions with too dense material on the surface.

In order to perform statistics on the size of the vesicles, AFM images were analysed using the 'Particle Analysis' tool of the instrument. For both the CG-NioP and CG-NioP-M samples, 20 different vesicles were analysed. The mechanisms of adsorption of vesicles on the substrate surface as well as the possible partial dehydration make the vesicles lose their original spherical shape resulting in spherical caps on the flat substrate surface [22], as depicted in the inset of Fig. 4(e). Each vesicle was analysed by evaluating the diameter D_{AFM} and the height h_{AFM} measured from the AFM morphology. Assuming that the adsorption and partial dehydration process modify the volume of the vesicle but not the surface area, the latter can be evaluated as the sum of the areas of the surface of the spherical cap $A_{cap} = \pi(D_{AFM}^2/4 + h_{AFM}^2)$ and of the base circle $A_{base} = \pi D_{AFM}^2/4$. Therefore, the equivalent diameter D_{eq} of a sphere with the same surface is given by:

$$D_{eq} = \sqrt{\frac{D_{AFM}^2}{2} + h_{AFM}^2} \qquad (2)$$

2.2.9. Brightfield microscopy

Samples of diluted CG-NioP and CG-NioP-M were held at room temperature in a 4-well Ibidi μ-slide, with a glass bottom especially conceived for microscopy purposes. The slide was adjusted into a motorized x-y translation stage, held in an Olympus IX73 inverted microscope, and illuminated by a conventional 100 W

halogen lamp through the condenser (N.A. 0.55). Transmitted light was collected by an UPLSAPO 100XO super-apochromat immersion oil objective (N.A. 1.4). Suitable optic elements projected the illuminated field of view onto a high-resolution high sensitivity CoolSNAP™ MYO CCD camera by Photometrics (1940x1460 imaging array, 4.54x4.54 μm pixel size, 20 MHz readout and 14 bit dynamic range) connected with the control workstation. The optical magnification converted the CCD pixel size at the imaging plane down to 45 nm.

The entire imaging setup, including the microscope, sample positioning, illumination and detection, was controlled via MetaMorph™ microscopy automation and image analysis software by Molecular Devices. Images of both the two samples were collected in streaming mode, at 36 fps, each image lasting 10 ms, for a total stream length of 1000 images, and stored as single timescan TIF files.

The time-stack stream files were processed via Fiji software bundle [23]. To emphasize the shape of the floating niosomes, time average images were subtracted to the respective time-stack streams. The particles traces appearing and disappearing on the focal plane were then isolated and the intensity profile measured along the trace. These curves were fitted with Lorentzians, a convenient approximation of the convolution between a hemisphere, the niosomes, and the overall microscope point spread function resulting from the combination of the condenser illumination and the objective collection. The profiles with the highest intensity and smaller full width at half maximum (FWHM) as obtained by the fit were then retained. More than 20 FWHM data were accumulated per each sample.

3. Results and discussion

Different perspectives to a given phenomenon help in sharpening the resolution in the parameter space. This approach is applied in characterizing the CG-mucin-niosomes complexes. The aim of the present paper is to obtain a unified description of chitosan coated niosomes/mucin interaction, taking advantage of the characteristics of each technique. This approach is able to highlight the same phenomenon but from different points of view and to give an overall idea of the final object.

291

292 *3.1. DLS*

293 The niosomal samples were tested for their size, ζ-potential, and
294 polydispersity index (PDI) using DLS measurements. CG-NioP niosomes bear
295 negative surface charge. This was due to the presence of the Span 20
296 surfactant and of a reduced amount of CG, which is insufficient to grant a
297 complete charge inversion on the vesicles, but that allows for a significant
298 interaction with the mucin. Higher amount of CG, would indeed produce
299 structures with different chemical-physical characteristics [11].
300 The size of empty CG-Nio is small (~170 nm), and it increases in presence of model
301 drug, but it does remain small enough for an efficient intranasal administration [1].
302 The interaction between mucin (the main component in mucus) and CG-NioP was
303 evaluated determining the differences in size and surface charge before and after
304 addition of mucin. The hydrodynamic diameter, ζ-potential, pH, and turbidity values
305 listed in Tab. 1 were all compatible with the same mucin-CG-NioP interaction
306 scheme. The values related to the CG-NioP-M that were always in between the
307 mucin and CG-NioP samples, while there were no evidences of mucin interacting
308 with uncoated samples (data not shown).

309

310

Sample	Vesicles diameter (10^2 nm)			ζ-Potential (mV)	PDI	Turbidity (arb. units)	pH
	DLS	AFM	BFM	DLS	DLS	Fluorimetry	
CG-NioP	2.0 ± 0.1	2.1 ± 0.3	2.2 ± 0.3	-46.3 ± 0.1	0.1	440.1	6.5
CG-NioP-M	2.6 ± 0.1	3.2 ± 0.1	3.0 ± 0.5	-30.0 ± 2.0	0.3	322.9	6.3
Mucin	16.2 ± 0.6		-	-15.6 ± 0.4	-	257.3	6.1

311

312 **Table 1.** Characteristics of CG-NioP, CG-NioP-M and Mucin. Vesicles diameter and
313 ζ-Potential are expressed as mean ± standard deviation of three measurements.
314 BFM data refer to deconvoluted average particle diameters.

315

316

317 The interaction between mucin and chitosan was a “non-specific” one, that includes

also a physical entanglement between the polymer and mucus layer, although CG-NioP bear negative ζ-potential values [24]. The PDI values of the mixtures were significantly higher than CG-NioP, due to the polydisperse system of the mixture, possibly as a consequence of the disordered assembly of the mucin layers onto the original niosomes surfaces. Size distribution by intensity curves for mucin alone, CG-NioP and CG-NioP-M were shown in Fig. 1 panel a. The bell-shaped size distribution curve of CG-NioP-M was located between the curves of mucin alone and CG-NioP, as a result of the adhesion of mucin on coated niosome samples; this behaviour suggests the successful formation of bigger aggregates and a complete mucin- CG-NioP due to the formation of the narrow curve of CG-NioP-M and the total disappearance of the mucin curve.

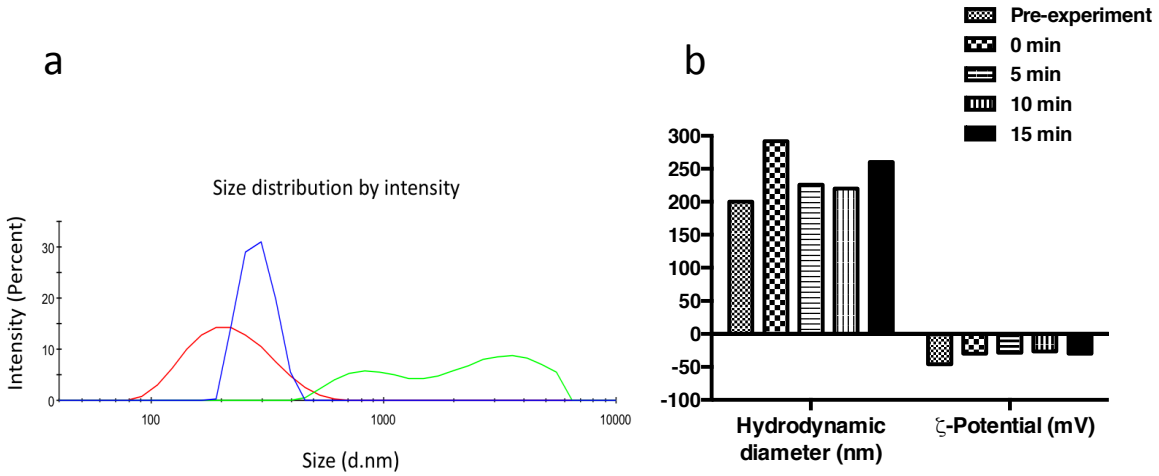

Figure 1. Panel a: Size distribution by intensity of CG-NioP (red), CG-NioP-M mixture (blue) and mucin solution (green). Panel b: Interaction kinetic and in vitro stability of complexes CG-NioP by DLS measurements.

To investigate the interaction kinetic of CG-NioP and mucin in terms of size and ζ-potential, measurements were carried out at different time intervals. In Fig. 1 panel b, the temporal evolution of these quantities as derived by DLS was shown. Already after 5 min, the particle size and the ζ-potential both increase, respect those reported in Table 1, up to a time average value around which the following respective measurements oscillate. It can be supposed that the interaction occurs immediately, and the obtained complexes remain stable during the time interval observed; this

aspect is important because it could predict a possible *in vivo* sample stability.

3.2. Spectrophotometry

The interaction between mucin and niosomes was evaluated by measuring the UV spectra of the supernatant after incubation and centrifugation. In Fig. 2: panel a the percentage of mucin in the precipitate is reported, measured as the difference between the total amount of mucin and the free mucin present in the supernatant. When only mucin was present in the suspension, the 50% precipitates after centrifugation, while when NioP were included in the solution, a little increase in the precipitated percent was noted, probably as a consequence of a mechanical interaction between niosomes and mucin. An almost complete precipitation of mucin occurred when CG-NioP were present in the suspension, because of the "non-specific" mucin interaction and a physical entanglement between the polymer and the mucus layer.

a

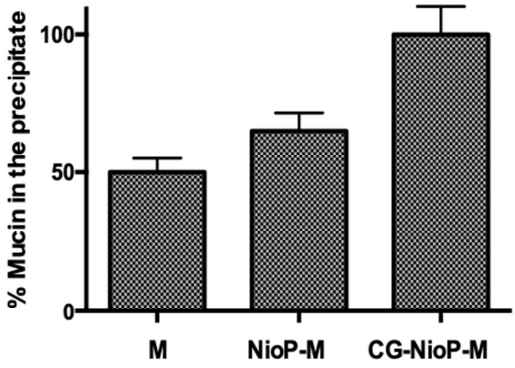

b

Sample	ΔA
CG-M	0.17
NioP-M	≅ 0
CG-NioP-M	0.15

Figure 2. Panel a: Mucoadhesive efficiency of niosome: mucin interaction evaluating the percent of precipitated mucin. Panel b: ΔA values as a measure of effectiveness interaction of CG-M, NioP-M and CG-NioP-M.

This technique is also useful to evaluate the mucoadhesion performance of CG-NioP expressed as difference in absorption (ΔA) (Fig. 2: panel b). The values obtained by mixing pure CG and mucin were reported.

This differential absorbance ΔA was able to provide information about the relevance of chitosan-mucin interaction in the overall process. The interaction between CG and mucin, considered as a reference for the purpose of this experiment, gives information about the maximum achievable interaction. This is the result of a balance between the interaction of anionic charges of mucin with positive ones on the polymeric chain and the competitive effect of ions and high ionic strength in the suspensions. After the addiction of mucin to NioP, no difference in absorption occurred, due to the absence of positive charges on the niosomal surface. CG-NioP presented a value of $\Delta A>0$, higher respect to our control that is NioP with mucin. Coated niosomes showed in fact a value of $\Delta A > 0$ comparable to the value obtained with CG-M, that were related to an interaction with mucin. In presence of CG, the niosomal adhesion performance was enhanced because of the best mucoadhesive properties due to the exposed charged groups on niosomal surface to external interactions. The CG present in the suspension was not completely free, as it was in the control suspension, because it was partially involved in the niosomal surface interaction and its ability to interact with mucin was depleted.

3.3. Fluorimetry

Bilayer characterization was carried out on NioP, CG-NioP and the mixture obtained after adding CG-NioP with mucin, respectively. Pyrene, a lipophilic probe, was located within the bilayer, and provides different information due to its different conformations inside the bilayer: monomers and excimers come up with different fluorescent spectra as depicted in Fig. 3.

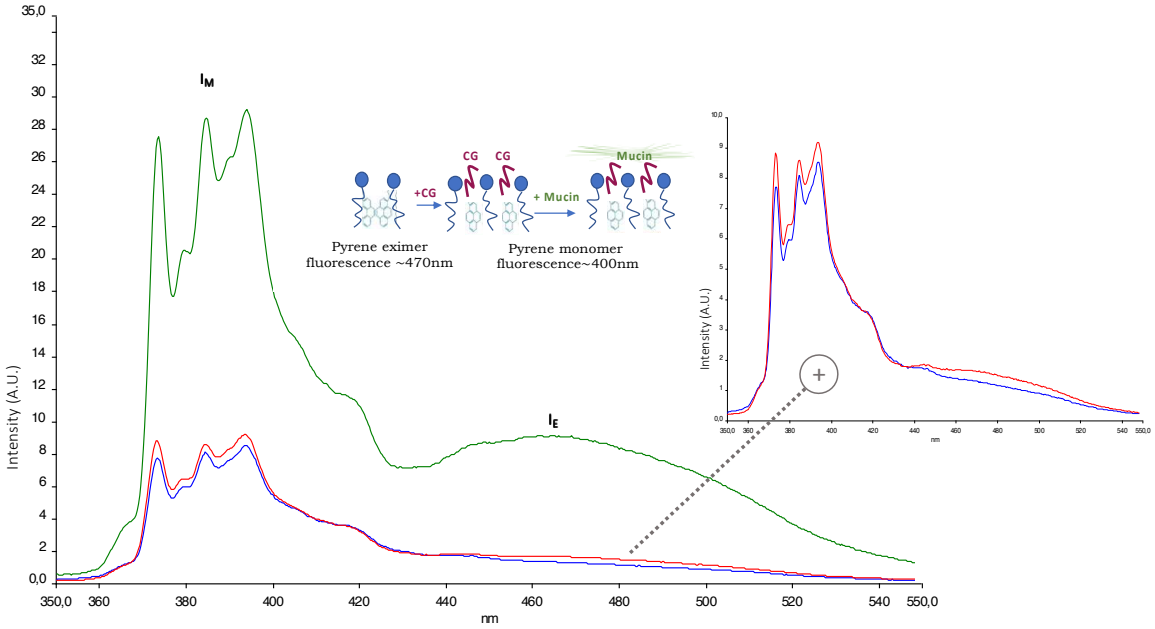

Figure 3. Pyrene emission spectrum (Ex: 330 nm; I_1= 373 nm; I_3= 385 nm; I_E= 464 nm) of samples: NioP (green), CG-NioP (red) and CG-NioP-M (blue).

Pyrene monomer exhibited a spectrum characterized with five emission peaks (from *I1* to *I5*) and pyrene excimer has only one peak (*IE*). The pyrene spectrum in NioP, in the absence of CG, shows peaks related to both monomer and excimer geometries, while when CG was added to the formulation, the disappearance of the excimer peak was observed. This was related not only to the external coating, but also to different interactions that might be responsible of a change in bilayer behaviour. The further addiction of mucin produces no dramatic change in the CG-NioP bilayer, as also indicated by the SAXS measurements discussed below. According to DLS data, the interaction between coated niosomes and mucin was responsible only for a dimensional increase of the complexes. The alternative and non conventional use of pyrene probe confirmed the external interaction between CG-NioP and mucin with no bilayer perturbation according to SAXS results.

3.4. AFM

In Fig. 4, the morphology of the CG-NioP and CG-NioP-M were shown. In Fig. 4(a) a region with too high density of deposited sample is evidenced and large amorphous blobs are visible, likely resulting from coalescence of several

vesicles. Single niosomes were visible on the surface of blobs as well as on the substrate. In order to obtain more accurate evaluation of vesicle size, regions with deposited material were chosen as reported in Fig. 4(c), (e) and (g), where several isolated niosomes with regular circular shape are clearly visible at different magnification.

High resolution images of CG-NioP vesicles, as the one reported in Fig. 4(i), show a niosomal granular surface. This is probably due to the convolution between the real shape of the molecules of the bilayer and the AFM tip which is spherical with nominal curvature radius less than 10 nm. In the analogous images of the CG-NioP-M, e.g., that reported in Fig. 4(b), in addition to large amorphous blobs and isolated vesicles, long filaments are visible, as evidenced by the arrow in Fig. 4(b). These filaments are peculiar of mucin, in fact they are not present in the sample CG-NioP. Images of the surface at different magnification of CG-NioP-M, (Fig. 4(d), (f) and (h)) show that vesicles possess regular circular shape and seem bigger than the corresponding samples without mucin. Indeed, statistical analysis on the height of niosomes confirms the increase of the mean vesicle height of CG-NioP-M respect to CG-NioP (i.e., from 20 ± 3 nm to 37 ± 3 nm). Analogously, the diameter increase of the vesicles on the substrates is observed (i.e., from 290 ± 40 nm to 450 ± 20 nm). Moreover, statistical analysis of D_{eq} of the niosomes evaluated using equation (2), and reported in Table 1, indicates the same increase of CG-NioP-M respect to CG-NioP (from 210 ± 30 nm to 320 ± 10 nm), in good agreement with results obtained by the other techniques.

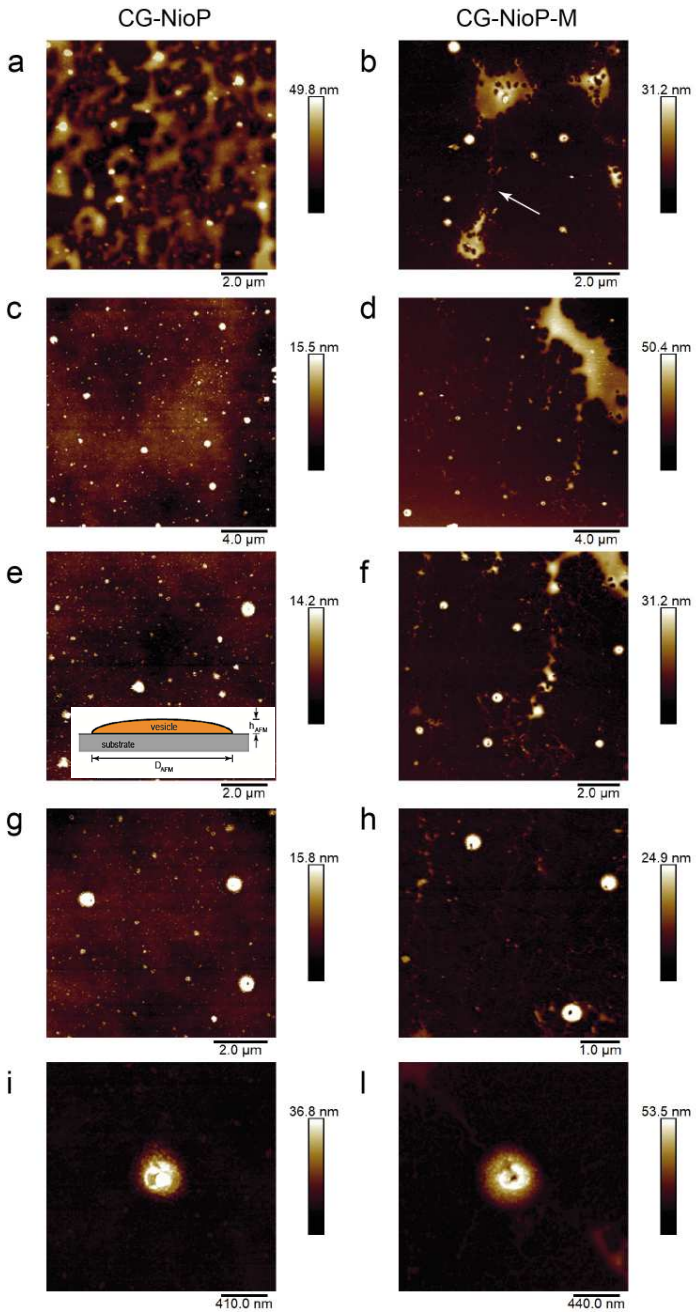

Figure 4. Microscopic images ad different magnification using AFM: (a,c,e,f,g,i) CG-NioP and (b,d,f,h,l) CG-NioP-M. In the inset in (e) the sketch of a vesicle adherent to the substrate is reported.

In this case, AFM technique, able to provide morphological and metrological information on nanocarriers; is also able to highlight the peculiar localization of mucin around the CG-NioP surface.

3.5. Brightfield microscopy

To image and to measure low absorption contrast nanometer sized suspended particles randomly moving in a solvent as a consequence of Brownian motion is a terrific challenge for modern microscopy [1, 25]. In the case of biocompatible particles, several constraints cannot be overcome: temperature and hydration could not be controlled to slow down the particle dynamics, as the physico-chemical environmental conditions strongly affect the particle character and behaviour; analogously, the viscosity of the solvent cannot be altered, as the chemistry of the niosomes is extremely sensitive.

At the same time, dynamics of nanometer sized bodies suspended in room temperature water (or any other equally viscous liquid) is fast (the diffusion constant could be estimated to be in the order of 10^{-12} m^2s^{-1}) and imaging time must be kept as short as possible, a trade-off with a photon devouring technique as microscopy is. On top of this, niosomes show a very low contrast with respect to the solvent, and the floating particles would appear as very weak perturbations of the homogeneous solvent background.

This set of restrictions was taken into account combining high spatial and temporal resolutions provided by brightfield microscopy imaging recorded at high framerate and high numerical aperture. The collected timestack movies show tiny spots, few pixels wide, swirling for fraction of seconds in the focal plane. A crop of the time sequence showing a particle entering and leaving the focal plane over a period of 220 ms is shown in Fig. 5: panel a.

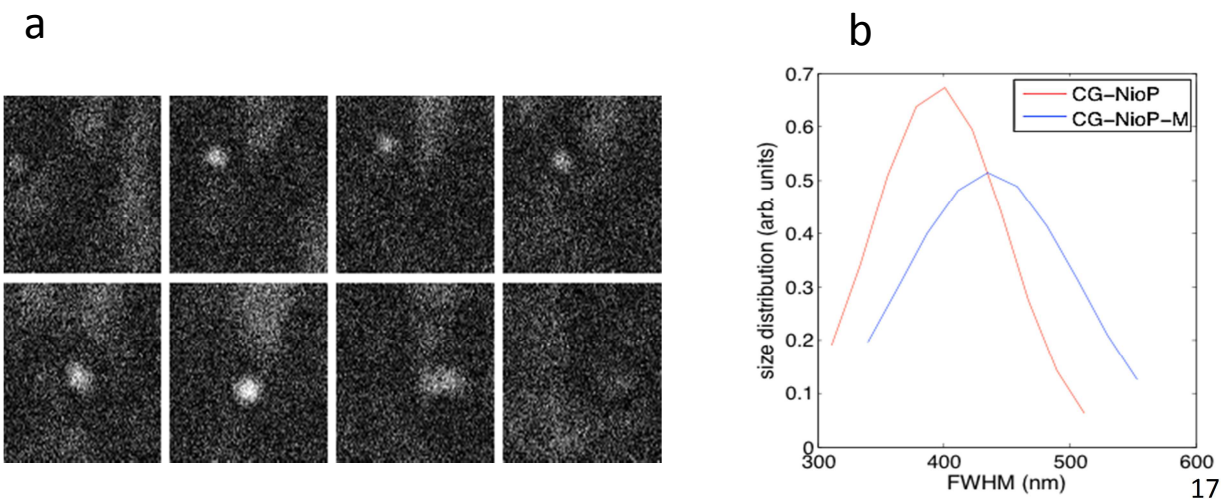

Figure 5. BFM experimental conditions of the images are as reported in section 2.2.9. Panel a: Time sequence montage of a 94x94 pixel crop timestack showing a CG-NioP-M particle entering and leaving the focal plane. Two next images are 28 ms apart, while the integration time per image is 10 ms. Panel b: Size distribution of CG-NioP and CG-NioP-M particles convoluted by the imaging point spread function, as determined via the procedure described in the text.

Several similar events were recorded per every sample and following the procedure described in the Materials and methods section, the full width half maximum (FWHM) distributions of these spots was obtained. The corresponding normal probability density functions for both the two niosome sets are depicted in figure Fig. 5: panel b.

The average sizes for CG-NioP and CG-NioP-M are (4.0±0.5) 10^2 nm and (4.4±0.7) 10^2 nm respectively. Of course, the FWHM determined by these measurements does not correspond to the actual particle size, since the particle projections on the focal plane are spread by the response of the imaging system to a point object. In principle, it is possible to estimate the shape of this response, namely the point spread function (PSF), but it is more convenient to measure it experimentally. In the case of our optical arrangement, the PSF can be approximated by a Lorentzian of 350 nm FWHM, and the deconvoluted average particle diameters for the two niosomes are reported in table 1.

3.6. SAXS

To investigate the internal structure of niosomes and their interaction with mucin, small angle X-ray scattering experiments on C, mucin and CG-NioP-M were carried out. In Fig. 6, left panel, SAXS spectra of CG-NioP (purple) and mucin (green). The intensity spectrum of mucin shows an intensity decay behavior characteristic for polymer chains in a good solvent $I(q) \div q^{-5/3}$. The spectrum of CG-NioP is dominated by the features of the Span-based shell. The intensity peak at q = 1.6 nm-1 is sign of an ordered structure. The q position corresponds to a characteristic distance $d = 2\pi/q$ between regularly arranged structures inside the niosomes. The presence of this peak is observed in multilamellar liposomes or Tween-based niosomes [5] and

the corresponding characteristic distance is the repetition distance within the multilamellar shell, d = thickness of the lamella plus thickness of the interlamellar water layer. In the present Span 20 based system, the observed distance is quite small, d = 3.8 nm, and just twice the length of a Span 20 molecule (about 2 nm). This result indicates that the shell of the niosomes is a multi-layered structure made of several Span layers in close contact, without the presence of any interlamellar water layer. In the right panel the intensity spectrum corresponding to the mixed 1:1 (w/w) niosome:mucin system is shown (blue) together with the reconstructed spectrum (red) obtained by simple addition of the two components, CG-NioP and mucin . The peak position still stays at q = 1.6 nm^{-1} revealing no dramatic change in the niosome internal structure in presence of mucin. Rather the measured intensity spectrum deviates from the reconstructed one in the low q region, corresponding to the large distances. This behaviour is sign of an interaction between mucin and the external surface of niosomes resulting in the formation of larger complexes.

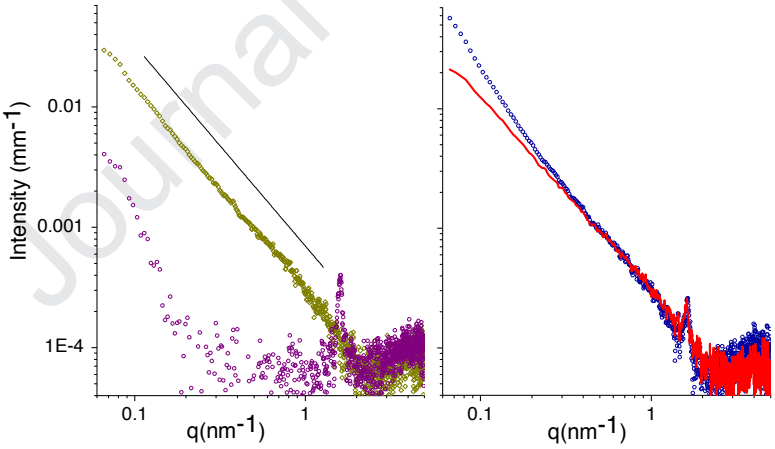

Figure 6. Left panel. SAXS spectra of CG-NioP (purple dots) and mucin (green diamonds) The black line represents the intensity decay behaviour I (q) ÷ $q^{-5/3}$. Right panel. CG-NioP-M intensity spectrum (blue dots) together with the reconstructed spectrum (red line) obtained by adding the contribution of the two (CG-NioP and mucin) components.

4. Conclusions

This study illustrates how these techniques can be used as valuable tools to obtain quantitative and qualitative information about the chitosan coated niosomes/mucin interaction. Dynamic light scattering (DLS), fluorimetric and spectrophotometric assays, small-angle X-ray scattering (SAXS), atomic force microscopy (AFM) and high speed brightfield microscopy (BFM) techniques proved to be highly complementary and parallel. Therefore their synergic combination allows for the characterization of a potential nanocarrier under development from the design of the vector, to the evolution of the structure upon encapsulation of the drug and interaction with biological barriers along the administration route, like mucin (Fig. 7: panel a). Some techniques are able to underline the increase of CG-NioP-M size respect to CG-NioP that confirm the phenomena of interaction. Although, as expected by different techniques, dimensions with different values are established, but the interaction sample/mucin is demonstrated by physical chemical properties variations that are, for all applied techniques always the same (≅ 30%). According to all techniques employed, the CG-Nio-P obtained from Span 20 surfactant shows in vitro mucoadhesive properties and the interaction mucin-sample would seem a superficial interaction, in fact, no change in the internal structure is observed by SAXS or fluorometric measurements. Moreover, the vesicle stability is maintained for 15 min, time of interaction with nasal mucosa after intranasal administration (Fig. 7: panel b).

However, further studies are needed to verify, in vivo, the improved bioavailability and the reduced drug clearance in nasal cavity respect to free drug.

These techniques, able to investigate physical-chemical features of nanocarriers and their mucin complexes, can be an essential tool to understand and refine information on the potential interaction between nanocarriers and biological environments, membranes and in vivo compartments.

a

CHARACTERIZATION TECHNIQUE	PARAMETERS ANALYSED
DLS	Particle size, size distribution and ζ-potential (surface charge)
AFM	Particle size and morphology
SAXS	Particle size and internal structure
BFM	Particle size and size distribution
Fluorometry	Turbidity, fluidity, microviscosity and polarity
Spectrophotometry	Mucin quantitative detection

b

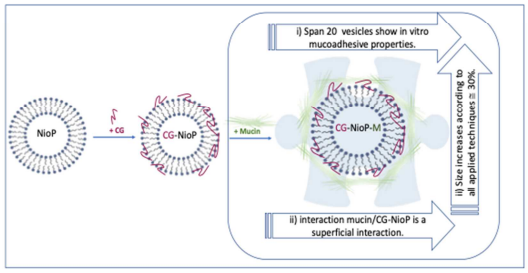

Figure 7. Panel a: Parameters evaluated by each technique to study niosome: mucin interaction. Panel b: Schematic representation of overall obtained results.

Acknowledgements

We thank ESRF for allocation of beamtime and Dr. A. Mariani for his assistance during SAXS experiments on ID02 beamline (ESRF). E.D.F. thanks BIOMETRA Department for in house support.

This work has been supported by Italian Ministry of Education, Universities and Research - Dipartimenti di Eccellenza - L. 232/2016 (Department of Drug Chemistry and Technologies, prof. Carafa and prof. Marianecci)

Founding

This research did not receive any specific grant from funding agencies in the public, commercial, or not-for-profit sectors.

References

[1] F. Rinaldi, L. Seguella, S. Gigli, P. Hanieh, E. Del Favero, L. Cantù, M. Pesce, G. Sarnelli, C. Marianecci, G. Esposito, inPentasomes: an innovative nose-to-brain pentamidine delivery blunts MPTP parkinsonism in mice, J. Control. Release 294 (2019) 17-26.

[2] D. Passeri, C. Dong, M. Reggente, L. Angeloni, M. Barteri, F.A. Scaramuzzo, F. De Angelis, F. Marinelli, F. Antonelli, F. Rinaldi, Magnetic

force microscopy: Quantitative issues in biomaterials, Biomatter 4 (2014) e29507.

[3] P.P. Mondal, A. Diaspro, Fundamentals of fluorescence microscopy: exploring life with light, Springer Science & Business Media (2013).

[4] M. Pluta, P. Maksymilian, Advanced light microscopy, Elsevier Amsterdam (1988).

[5] C. Marianecci, L. Di Marzio, E. Del Favero, L. Cantù, P. Brocca, V. Rondelli, F. Rinaldi, L. Dini, A. Serra, P. Decuzzi, Niosomes as drug nanovectors: multiscale pH-dependent structural response, Langmuir 32 (2016) 1241-1249.

[6] E. Gavini, G. Rassu, L. Ferraro, A. Generosi, J.V. Rau, A. Brunetti, P. Giunchedi, A. Dalpiaz, Influence of chitosan glutamate on the in vivo intranasal absorption of rokitamycin from microspheres, J. Pharm. Sci. 100 (2011) 1488-1502.

[7] L. Illum, P. Watts, A. Fisher, M. Hinchcliffe, H. Norbury, I. Jabbal-Gill, R. Nankervis, S. Davis, Intranasal delivery of morphine, J. Pharmacol. Exp. Ther. 301 (2002) 391-400.

[8] L. Illum, Nasal drug delivery—recent developments and future prospects, J. Control. Release 161 (2012) 254-263.

[9] E.B. Manaia, M.P. Abuçafy, B.G. Chiari-Andréo, B.L. Silva, J.A.O. Junior, L.A. Chiavacci, Physicochemical characterization of drug nanocarriers, Int. J. Nanomed. 12 (2017) 4991.

[10] F. Rinaldi, P.N. Hanieh, C. Marianecci, M. Carafa, DLS Characterization of Non-Ionic Surfactant Vesicles for Potential Nose to Brain Application, Nanosci. Nanometr. 1 (2015) 8-14.

[11] F. Rinaldi, P.N. Hanieh, L.K.N. Chan, L. Angeloni, D. Passeri, M. Rossi, J.T.-W. Wang, A. Imbriano, M. Carafa, C. Marianecci, Chitosan Glutamate-Coated Niosomes: A Proposal for Nose-to-Brain Delivery, Pharmaceutics 10 (2018) 38.

[12] C. Aguzzi, G. Sandri, C. Bonferoni, P. Cerezo, S. Rossi, F. Ferrari, C. Caramella, C. Viseras, Solid state characterisation of silver sulfadiazine loaded on montmorillonite/chitosan nanocomposite for wound healing, Colloids Surf. B Biointerfaces 113 (2014) 152-157.

[13] S. Sennato, F. Bordi, C. Cametti, M. Diociaiuti, P. Malaspina, Charge patch attraction and reentrant condensation in DNA–liposome complexes, BBA-Biomembranes 1714 (2005) 11-24.

[14] P.T. Wong, S.H. Wang, S. Ciotti, P.E. Makidon, D.M. Smith, Y. Fan, C.F. Schuler IV, J.R. Baker Jr, Formulation and characterization of nanoemulsion intranasal adjuvants: effects of surfactant composition on mucoadhesion and immunogenicity, Mol. Pharmaceut. 11 (2013) 531-544.

[15] A. Sosnik, J. das Neves, B. Sarmento, Mucoadhesive polymers in the design of nano-drug delivery systems for administration by non-parenteral routes: a review, Prog. Polym. Sci. 39 (2014) 2030-2075.

[16] T. Klemetsrud, H. Jonassen, M. Hiorth, A.-L. Kjøniksen, G. Smistad, Studies on pectin-coated liposomes and their interaction with mucin, Colloids Surf. B Biointerfaces 103 (2013) 158-165.

[17] Y.A. Albarkah, R.J. Green, V.V. Khutoryanskiy, Probing the Mucoadhesive Interactions Between Porcine Gastric Mucin and Some Water-Soluble Polymers, Macromol. Biosci. 15 (2015) 1546-1553.

[18] E. McClean, L. McGrath, G. Archbold, Comparison of two fluorescent probes for the measurement of erythrocyte membrane fluidity in renal dialysis patients, Irish J. Med. Sci. 164 (1995) 289-292.

[19] K. Zachariasse, Microviscosity measurements in micelles and phospholipids, Berich. Bunsen. Gesell. 82 (1978) 950-950.

[20] C. Ingallina, F. Rinaldi, A. Bogni, J. Ponti, D. Passeri, M. Reggente, M. Rossi, A. Kinsner-Ovaskainen, D. Mehn, F. Rossi, Niosomal approach to brain delivery: Development, characterization and in vitro toxicological studies, Int. J. Pharmaceut. 511 (2016) 969-982.

[21] G. Sandri, S. Motta, M.C. Bonferoni, P. Brocca, S. Rossi, F. Ferrari, V. Rondelli, L. Cantù, C. Caramella, E. Del Favero, Chitosan-coupled solid lipid nanoparticles: tuning nanostructure and mucoadhesion, Eur. J. Pharm. Biopharm. 110 (2017) 13-18.

[22] O. Teschke, E. De Souza, Liposome structure imaging by atomic force microscopy: verification of improved liposome stability during adsorption of multiple aggregated vesicles, Langmuir 18 (2002) 6513-6520.

[23] C.T. Rueden, J. Schindelin, M.C. Hiner, B.E. DeZonia, A.E. Walter, E.T. Arena, K.W. Eliceiri, ImageJ2: ImageJ for the next generation of scientific image data, BMC bioinformatics 18 (2017) 529.

[24] M.I. Adamczak, Ø.G. Martinsen, G. Smistad, M. Hiorth, Polymer coated mucoadhesive liposomes intended for the management of xerostomia, Int. J. Pharmaceut. 527 (2017) 72-78.

[25] D. Coglitore, S.P. Edwardson, P. Macko, E.A. Patterson, M. Whelan, Transition from fractional to classical Stokes–Einstein behaviour in simple fluids, Roy. Soc. Open Sci. 4 (2017) 170507.

Highlights

- Physical-chemical characterization of niosomes/mucin interaction.
- Different, non conventional and complementary techniques to perform analytical characterization.
- DLS, AFM, BFM, Spectrophotometric techniques.
- SAXS, Fluorimetric techniques.
- No change of internal niosomal structure, superficial mucin interaction.

Conflicts of Interest: The author declares no conflict of interest.